EFFECT OF ANNEALING TEMPERATURE ON THE STRUCTURAL AND THERMOELECTRIC PROPERTIES OF $CuFeS_2$ NANOPARTICLES PREPARED BY THE HYDROTHERMAL METHOD

EFECTO DE LA TEMPERATURA DE RECOCIDO SOBRE LAS PROPIEDADES ESTRUCTURALES Y TERMOELÉCTRICAS DE LAS NANOPARTÍCULAS DE $CuFeS_2$ PREPARADAS POR EL MÉTODO HIDROTERMAL

Safaa H. Ali[1*], Saad S. Mohammed[2]

[1] Al-Shatrah University, College of Education, Department of Physics, Al-Shatrah, 64007, Iraq.
[2] University of Thi-Qar, College of Science, Department of Chemistry, Nasyriah, 64001, Iraq.

(Recibido: may./2024. Aceptado: oct./2024)

Abstract

The current study described precise and simple hydrothermal method used to synthesize $CuFeS_2$ nanoparticles. The thermoelectric properties of $CuFeS_2$ nanoparticles were studied under different conditions of annealing treatment. The phase structure, functional groups, and thermal stability of the $CuFeS_2$ nanoparticles samples were analyzed via X-ray diffractometer (XRD), Fourier transform infrared spectroscopy (FT-IR), and thermogravimetric analysis (TGA). The X-ray diffraction (XRD) results of the synthesized nanoparticles closely matched the $CuFeS_2$ chalcopyrite patterns. FT-IR measurements confirmed the presence of the characteristic S-O, Fe-S, and O-H groups in the structure of the prepared nanoparticles. The TGA results indicate that the $CuFeS_2$ nanoparticles are thermally stable below 650°C. The scan electron microscope (SEM) measurements revealed that the particle size of all the samples was less than 100 nm after the annealing treatment. The optical measurements showed

* safaa.ali@shu.edu.iq doi: https://doi.org/10.15446/mo.n70.114275

that the absorbance edges of the $CuFeS_2$ samples shifted to longer wavelengths after the annealing treatment. The thermoelectric measurements indicated that the annealing treatment modulated the electrical conductivity, Seebeck coefficient, power factor, and thermal conductivity of the $CuFeS_2$ samples.

Keywords: annealing, $CuFeS_2$, nanoparticles, Seebeck coefficient, thermoelectric.

Resumen

En este estudio, se sintetizaron nanopartículas de $CuFeS_2$ mediante el método hidrotermal. Las propiedades termoeléctricas se estudiaron bajo diferentes condiciones de tratamiento térmico. La estructura de fases, los grupos funcionales y la estabilidad térmica de las muestras de $CuFeS_2$ se analizaron mediante difractometría de rayos X (XRD), espectroscopia infrarroja por transformada de Fourier (FT-IR) y análisis termogravimétrico (TGA). Se descubrió que los resultados de la difracción de rayos X (DRX) de las nanopartículas sintetizadas coinciden estrechamente con los patrones de calcopirita $CuFeS_2$. Las mediciones de FT-IR confirman la presencia de grupos S-O, Fe-S y O-H en la estructura de las nanopartículas preparadas. Los resultados del análisis TGA indican que las nanopartículas de $CuFeS_2$ son térmicamente estables por debajo de 650 °C. Las mediciones SEM mostraron que el tamaño de partícula de todas las muestras estaba por debajo de 100 nm después del tratamiento de recocido. Las mediciones ópticas mostraron que los bordes de absorbancia de las muestras de $CuFeS_2$ cambiaron a longitudes de onda más largas después del tratamiento de recocido. Las mediciones termoeléctricas indicaron que el tratamiento de recocido modula la conductividad eléctrica, el coeficiente de Seebeck, el factor de potencia y la conductividad térmica de las muestras de $CuFeS_2$.

Palabras clave: recocido, $CuFeS_2$, nanopartículas, coeficiente Seebeck, termoeléctrico.

Introduction

During the use of solar, fossil, and electric energy, some heat energy is released as waste [1]. In thermoelectric devices, part of the generated heat can be converted directly to electrical energy to power the system and can also be used to cool the system, ensuring its operational stability [2–5]. Thermoelectric technology is considered an eco-friendly solution for the global energy crisis, as it enables solid-state conversion between electricity and heat [1, 2]. Different thermoelectric materials such as PbTe, silicides, super ionic materials, and half-Heusler materials are used in power generation applications [3–8]. The conversion efficiency of thermoelectric materials is dominated by the figure of merit ($ZT = S2\sigma T/\kappa$), where $S2\sigma$, σ, S, T, and κ represent the power factor, electrical conductivity, Seebeck coefficient, absolute temperature, and total thermal conductivity, respectively [9]. To improve the ZT value, we must optimize these parameters because they are strongly correlated with each other [10–13]. Increasing the ZT value, several methods have been utilized, such as band structure engineering, carrier concentration (n) optimization, nanostructure engineering, grain boundary engineering, and phonon engineering [14–26]. Chalcopyrite ($CuFeS_2$) is a ternary compound that is well-known as a semiconductor with antiferromagnetic properties. $CuFeS_2$ has a high Néel temperature of 550 °C, a narrow band gap (0.5–0.6 eV), and innovative electrical, magnetic, and optical properties [27–31]. It has wide applications, including thermoelectric devices, cathodes of lithium-ion batteries, and solar cells [31–33]. Different methods have been explored for the synthesis of various types of $CuFeS_2$, such as hydrothermal synthesis [34, 35], solvothermal processes [36, 37], thermal decomposition [38], and spark plasma sintering [31]. Annealing can alter the optical, photoelectrochemical, electrical, crystallinity, structural, and mechanical properties of different types of materials [39–45].

In this work, the $CuFeS_2$ compound was prepared via a hydrothermal method. The synthesized compound was subjected

to annealing treatment at different temperatures. The effects of the annealing treatments on the structure and thermoelectric properties of the $CuFeS_2$ compound were investigated.

Materials and Methods

Chemicals

Polyethylene glycol, cupric chloride, iron sulfate, polyvinylpyrrolidone, and thiourea were purchased from Sigma Aldrich and used as received.

Preparation of the $CuFeS_2$ Nanoparticles

To prepare the $CuFeS_2$ nanoparticles, 0.7654, 0.6785, and 1.058 g of $CuCl_2$, $SC(NH_2)_2$, and $FeSO_4$ were separately dissolved in 20, 10, and 10 ml of deionized water, respectively. The three obtained solutions were subsequently mixed together and stirred for 30 min. With respect to the $CuCl_2$ reagent, a 1:1 mole ratio of polyvinylpyrrolidone was added to the solution and stirred for 10 min. The resulting solution was subsequently mixed with 80 ml of polyethylene glycol. The resulting solutions were then separately transferred to an autoclave, placed in an oven, and subjected to heat treatments at 200 °C (S1), 250 °C (S2), and 300 °C (S3) for 24 hours. The resulting samples were subsequently washed with ethanol, HCl, and distilled water, and finally dried for 24 h at 60 °C.

Characterization

XRD analysis was conducted with a Bruker D8 X-ray diffractometer to identify the purity, phase composition, and diffraction patterns of the samples. Fourier transform-infrared (FT-IR) spectra were measured via a Shimadzu Varian 4300 spectrophotometer, with KBr pellets, at room temperature. Thermogravimetric analysis (TGA) was performed using a Netzsch STA449F3A-1517-M instrument. Surface morphology images were obtained via a

JEOL scanning electron microscope (model 6610OLV). The optical properties were analyzed via UV-Vis spectroscopy (1601 PC) in the range of 400-900 nm. The electrical conductivity and Seebeck coefficient were measured via a ZEM-3 instrument from Ulvac Riko, Inc. The measurements were conducted in a helium atmosphere at temperatures ranging from 300 to 650 K. The thermal conductivity was characterized via the laser technique by a Netzsch LFA427. The Hall effect was measured at room temperature via a Lakeshore 7707 Hall analyzer.

Results and Discussion

Figure 1 shows the X-ray diffraction patterns of $CuFeS_2$ samples (S1, S2, and S3) prepared at different temperatures. The XRD patterns show characteristic diffraction peaks that correspond to the 112, 200, 004, 220, 204, 312, and 116 lattice planes of $CuFeS_2$ (JCPDS no. 35-0752). Additionally, the calculated crystallite sizes from the Scherrer formula for the synthesized samples (Table 1) were 55.14, 73.49, and 86.83 nm for the S1, S2, and S3 samples, respectively. According to the XRD analysis, all the samples perfectly matched the $CuFeS_2$ chalcopyrite phase, and the annealing treatment enhanced the crystallite growth.

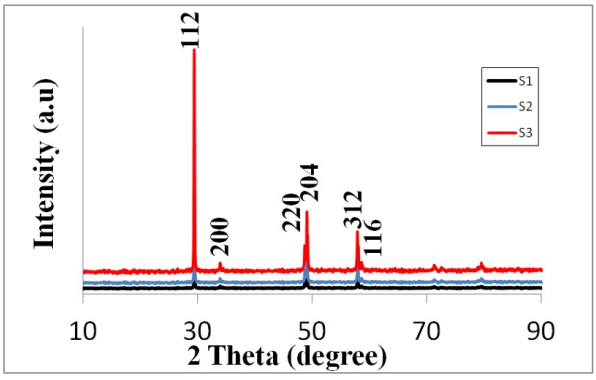

FIGURE 1. *XRD patterns of $CuFeS_2$ samples*

Sample	Peak position 2θ	FWHM	Dp (nm)	Uncertainty ΔD_p (nm)
S1	29.40	0.15556	55.14	± 0.68
S2	29.40	0.11673	73.49	± 1.21
S3	29.41	0.09879	86.83	± 1.68

TABLE 1. *Calculated crystallite size (D_p) of the $CuFeS_2$ samples*

FT-IR measurements were employed to study the functional groups of the samples, and the obtained spectra are shown in Figure 2. The peaks at 672 and 795 cm^{-1} are assigned to S–O bending and Fe–S vibrations, respectively. Additionally, S–O bending and stretching can be observed at 1118 and 1632 cm^{-1}, respectively. In addition, the peaks in the region (3000–3700 cm^{-1}) can be attributed to O–H vibrations of hydroxyl group stretching.

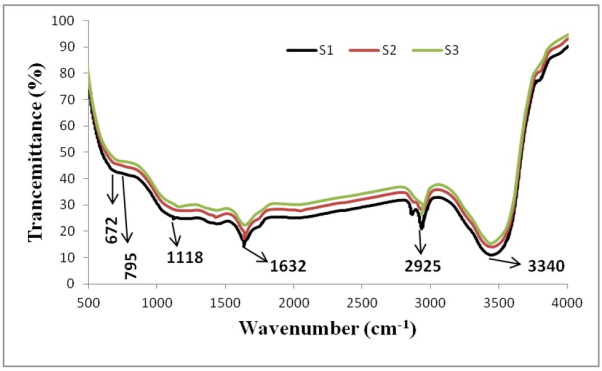

FIGURE 2. *FT-IR spectra of the $CuFeS_2$ samples*

The thermal stability of the $CuFeS_2$ samples was also studied via thermogravimetric analysis (TGA). As shown in Figure 3, the provided TGA curve displayed distinct mass loss events across various temperature ranges. Initially, a minor decrease in mass was observed from 0 °C to approximately 150 °C, which was attributed to the evaporation of adsorbed moisture or the release of physically adsorbed water from the nanoparticle surface. This was followed by a gradual mass decrease from approximately 150 °C to 400 °C, likely due to the decomposition or desorption of organic components and solvents employed during synthesis. The mass fluctuated slightly between 400 °C and 600 °C, indicating a region of relative thermal stability, with minor fluctuations possibly

resulting from slight rearrangements or phase transitions within the material. A significant mass loss occurred between approximately 600 °C and 800 °C, suggesting the decomposition of the $CuFeS_2$ nanoparticles into FeS and CuS. This temperature range marked a critical transition, indicating the thermal stability limit of the nanoparticles. In addition, from approximately 800 °C to 1000 °C, a further but less significant mass decrease was recorded, likely due to the continued oxidation of residual sulfides or the decomposition of the remaining thermally unstable phases. The slight plateau observed above approximately 900 °C indicated the formation of a more stable phase, which was presumed to be an oxide.

In the final temperature range, between 1000 °C and 1200 °C, the mass remained relatively stable, suggesting that all thermally unstable phases had decomposed, and that a stable oxide phase had formed. This phase appeared resistant to further thermal decomposition or oxidation.

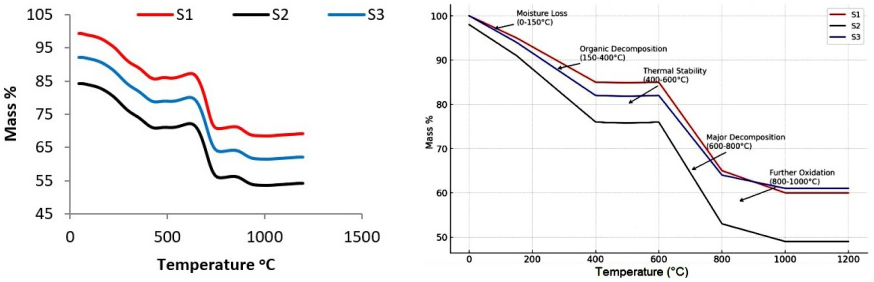

(a) *(b)*

FIGURE 3. *TGA curves of the $CuFeS_2$ samples*

The surface morphology of the $CuFeS_2$ samples is depicted in Figure 4. Scanning electron microscopy (SEM) images reveal crucial details about the size and shape of the annealed particles. According to SEM measurements, the average particle size for all the samples was less than 100 nm. The SEM images clearly show that the $CuFeS_2$ samples exhibit a highly agglomerated, homogeneous, nanosized spherical morphology. Furthermore, there is a slight increase in the average particle size within the nanometer range as the annealing temperature increases.

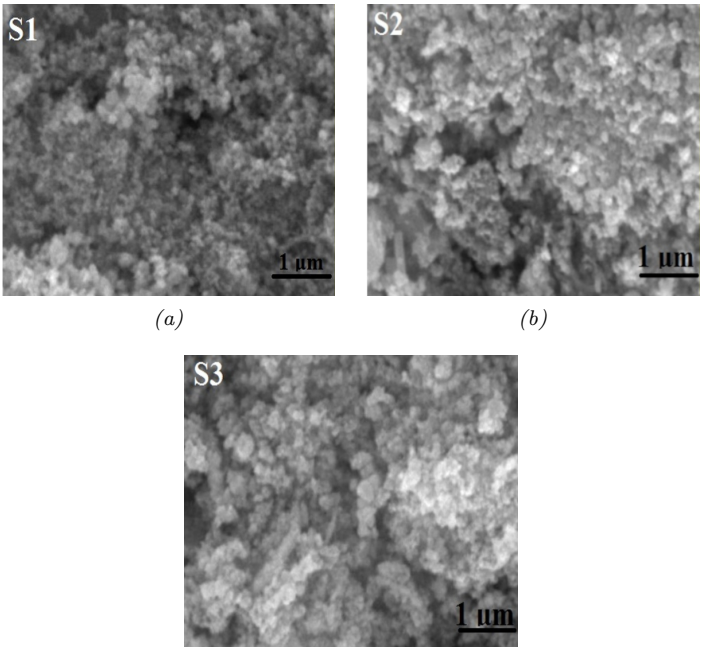

(a) (b)

(c)

FIGURE 4. *SEM images of the $CuFeS_2$ samples*

Figure 5 displays the absorption spectra of the $CuFeS_2$ samples at each annealing temperature.

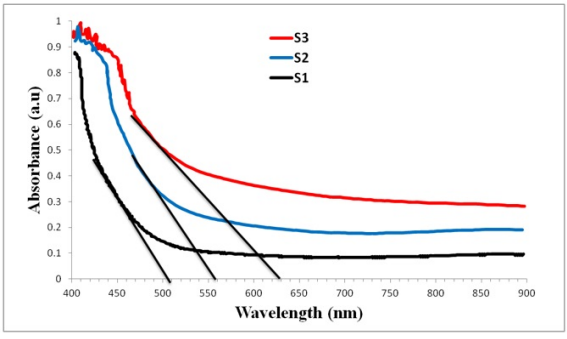

FIGURE 5. *$CuFeS_2$ absorption spectrum*

The energy gap (E_g) was calculated according to the Planck relation:

$$E_g = h\frac{C}{\lambda}$$

where h, C, and λ are the Planck constant, light velocity, and absorption edge (nm) respectively. The annealing treatment clearly improved the absorbance of $CuFeS_2$ and shifted the absorbance edge to the visible region. Similarly, the energy gap decreased as a result of the annealing treatment, and the calculated values were 2.43 eV, 2.21 eV, and 1.96 eV for the S1, S2, and S3 samples, respectively.

The electrical transport properties of all the samples at room temperature are listed in Table 2. The electrical conductivity (Figure 6) of the $CuFeS_2$ samples decreases with increasing annealing temperature, which can be related to a decrease in the carrier concentration. As the annealing temperature increased, the $CuFeS_2$ nanoparticles likely underwent significant structural and compositional transformations. Higher temperatures can promote the diffusion and migration of atoms, leading to the growth of larger crystalline domains and a reduction in defects and grain boundaries. These changes can decrease the number of free carriers, as grain boundaries and defects often act as carrier traps or sources of ionized impurities.

Parameter	**S3**	**S2**	**S1**
Seebeck coefficient (μVK^{-1})	-146.8	-169.9	-217.8
Electrical conductivity (10^4 S m^{-1})	1.91	1.71	1.31
Thermal conductivity ($Wm^{-1}K^{-1}$)	1.71	3.19	4.41
Carrier concentration ($10^{19}\,cm^{-3}$)	97.9	39.8	17.1
Carrier mobility ($cm^2\,V^{-1}\,S^{-1}$)	1.21	2.69	4.71

TABLE 2. *Transport parameters of the $CuFeS_2$ samples at room temperature*

Figure 7 displays the Seebeck coefficients of the $CuFeS_2$ nanoparticles. The negative Seebeck coefficient values indicate that all samples are n-type semiconductors, where electrons are the charge carriers. Additionally, the values of the Seebeck coefficients decreased with increasing annealing temperature. The magnitude of the Seebeck coefficient increased by approximately 27.59 % when the annealing temperature was increased from 200 °C to 250 °C, and by approximately 21.62 % when the annealing temperature was increased from 250 °C to 300 °C.

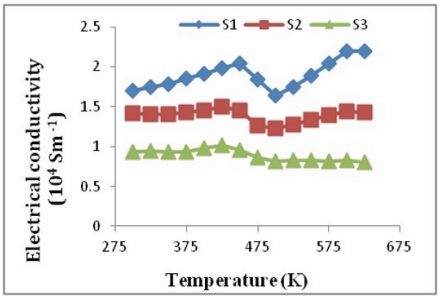

FIGURE 6. *Electrical conductivity of the $CuFeS_2$ samples*

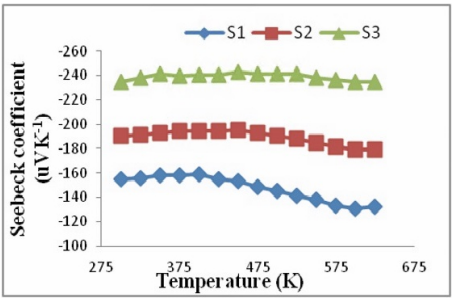

FIGURE 7. *Seebeck coefficient of the $CuFeS_2$ samples*

The calculated power factor $\alpha 2\sigma$ of all the $CuFeS_2$ samples is shown in Figure 8. The power factor values indicate that the sample annealed at a higher temperature (S3) had the highest power factor compared with the sample annealed at a lower temperature (S1).

Figure 9 shows the total thermal conductivity for all the $CuFeS_2$ samples. The investigation of the $CuFeS_2$ nanoparticles revealed that the total thermal conductivity increased with increasing annealing temperature. This behavior was likely due to several contributing factors such as crystallinity, reduced defects, and larger grain sizes within the $CuFeS_2$ nanoparticles at high annealing temperatures.

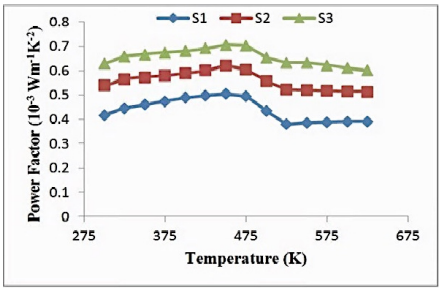

FIGURE 8. *Power factor of the $CuFeS_2$ samples*

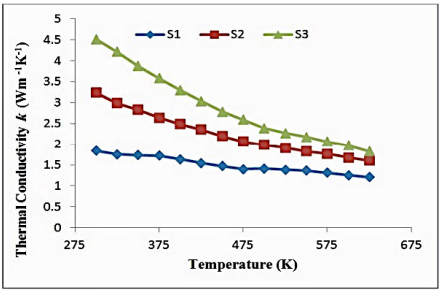

FIGURE 9. *Total thermal conductivity of the $CuFeS_2$ samples*

Figure 10 displays the obtained figure of merit ZT for the $CuFeS_2$ samples. All the $CuFeS_2$ samples clearly show a similar ZT trend, with the S1 sample having the highest ZT values, whereas the

S3 sample has the lowest values. However, the lower thermal conductivity and superior electrical performance of the S1 sample annealed at 200 °C were likely responsible for its higher ZT value than those of the samples annealed at 250 °C (S2) and 300 °C (S3). The lower thermal conductivity would minimize heat loss, thereby enhancing the thermal gradient required for thermoelectric power generation. Moreover, the superior electrical performance, which could be attributed to the optimal carrier concentration and reduced defect density, would have contributed to a higher power factor. The combination of these factors resulted in a more favorable balance between electrical conductivity, the Seebeck coefficient, and thermal conductivity, leading to the highest ZT value for the sample annealed at 200 °C.

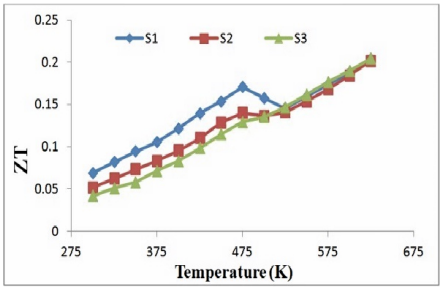

FIGURE 10. *Merit figure ZT for the CuFeS2 samples*

Conclusion

In summary, we synthesized $CuFeS_2$ nanoparticles via a hydrothermal method at various annealing temperatures. The influences of heat treatment on the structure and thermoelectric properties of the synthesized $CuFeS_2$ nanoparticles were elucidated via various characterization methods. XRD measurements confirmed that the $CuFeS_2$ crystallite size ranged from 55 to 86 nm, with the annealing temperature enhancing the growth of the crystallites. The $CuFeS_2$ structural and functional groups investigated by FT-IR spectroscopy confirmed the existence of Fe-S, O-H, and S-O bonds in all the samples. The scanning electron microscopy (SEM) results showed that samples annealed

at higher temperatures have larger particle sizes. The annealing treatment also enhances the optical properties of $CuFeS_2$ samples and decreases the energy gap values. The thermoelectric results indicate that heat treatment improves the power factor and thermal conductivity while reducing the Seebeck coefficient and electrical conductivity. All the $CuFeS_2$ samples exhibit a similar ZT trend, with the highest ZT values recorded for the sample annealed at a low temperature.

Conflict of Interest

The authors declare no conflict of interest.

Acknowledgments

This work did not receive any funds from any organization and was funded by the authors'private money. The authors gratefully acknowledge Thi-Qar University and Al-Shatrah University for providing some research facilities.

References

[1] L. E. Bell, Science **321**, 1457 (2008).
[2] F. J. DiSalvo, Science **285**, 703 (1999).
[3] W. Liu, H. Kim, and et al., Scripta Materialia **111**, 3 (2016).
[4] W. He, G. Zhang, and et al., Applied Energy **143**, 1 (2015).
[5] I. Chowdhury, R. Prasher, and et al., Nat. Nanotechnol. **4**, 235 (2009).
[6] D. Beretta, N. Neophytou, and et al., Mater. Sci. Eng. R: Rep. **138**, 100501 (2019).
[7] Y. Wang, L. Yang, and et al., Adv. Mat. **31**, 1807916 (2019).
[8] G. Babu and X. Shajan, J. Mater. Sci.: Mater. Electron. **34**, 2286 (2023).
[9] I. Cohen, M. Kaller, and et al., J. Mater. Chem. C **3**, 9559 (2015).

[10] L. Fang, J. Liu, and et al., Appl. Phys. Lett. **97**, 242501 (2010).
[11] G. Guttmann, D. Dadon, and et al., J. Appl. Phys. **118**, 065102 (2015).
[12] Y. Vahidshad, S. Mirkazemi, and et al., J. Nanstruct. **7**, 284 (2017).
[13] W. Liu, L. Yang, and et al., Adv. Mater. **32**, 1905703 (2020).
[14] B. Karuppannan, J. Sturgeon, and et al., SN Appl. Sci. **2**, 1931 (2020).
[15] J. R. Sootsman and et al., Angewandte Chemie Int. Ed. **48**, 8616 (2009).
[16] R. Akram, J. Akhtar, and et al., J. Mater. Sci.: Mater. Electron. **32**, 24619 (2022).
[17] S. Aoudj, A. Khelifa, and et al., Chem. Eng. J. **267**, 153 (2015).
[18] H. Dhiflaoui, N. Jaber, and et al., Thin Solid Films **638**, 201 (2017).
[19] T. Zhu, Y. Liu, and et al., Adv. Mater. **29**, 1605884 (2017).
[20] C. Kim, D. Lopez, and et al., J. Mater. Chem. A **7**, 791 (2019).
[21] L. Zhao, H. Wu, and et al., Energy Environ. Sci. **6**, 3346 (2013).
[22] Y. Pei, X. Shi, and et al., Nature **473**, 66 (2011).
[23] M. Hong, Z. Chen, and et al., J. Mater. Chem. A **5**, 10713 (2017).
[24] P. Zong, R. Hanus, and et al., Energy Environ. Sci. **10**, 183 (2017).
[25] S. Kim, K. H. Lee, and et al, Science **348**, 109 (2015).
[26] G. Han, Z. Chen, and et al., Small **10**, 2747 (2014).
[27] L. Huang, J. Lu, and et al., J. Mater. Chem. A **8**, 1394 (2020).
[28] A. Umar, R. Kumar, and et al., J. Alloys Compd. **648**, 46 (2015).
[29] M. Hong, Z. Chen, and et al., Nano Energy **20**, 144 (2016).
[30] A. Jafari, S. Shayesteh, and et al., J. Magn. Magn. Mater. **379**, 305 (2015).
[31] A. Ashfaq, A. Ali, K. Mahmood, and et al., Ceram. Int. **47**, 35356 (2021).
[32] D. K. Muthee and B. F. Dejene, Heliyon **7**, e07269 (2021).

[33] R. Suresh, V. Ponnuswamy, and R. Mariappan, Appl. Surf. Sci. **273**, 457 (2013).

[34] S. Singh, N. Kumar, and et al., J. Supercond. Nov. Magn. **27**, 821 (2014).

[35] L. Attou, B. Jaber, and et al., Mediterr. J. Chem. **7**, 308 (2018).

[36] S. Hasan and B. Azhdar, Ceram. Int. **49**, 5371 (2023).

[37] A. Zak, M. Abrishami, and et al., Ceram. Int **37**, 393 (2011).

[38] B. Shah, S. Chaki, and et al., Mater. Sci. Semicond. Process. **179**, 108495 (2024).

[39] U. Rehman, J. Jacob, and et al., Ceram. Int **46**, 20496 (2020).

[40] M. Khan, J. Zhai, and et al., ChemPhysMater **2**, 207 (2023).

[41] Y. Muddassir, S. Tahir, and et al., Appl. Phys. A **127**, 457 (2021).

[42] X. Meng, X. Jing, and et al., ACS Appl. Nano Mater. **7**, 8175 (2024).

[43] U. Rehman, K. Mahmood, and et al., Mater. Chem. Phys. **279**, 125765 (2022).

[44] M. Moorthy, P. Govindaraj, and et al., ACS Appl. Energy Mater. **7**, 2008 (2024).

[45] S. Ali, S. Mohammed, and et al., Chem. Chem. Technol. **16**, 639 (2022).